J. Biochem. 2011;150(6):659–669 doi:10.1093/jb/mvr103

JB THE JOURNAL OF BIOCHEMISTRY

High resolution X-ray crystal structures of L-phenylalanine oxidase (deaminating and decarboxylating) from *Pseudomonas* sp. P-501. Structures of the enzyme-ligand complex and catalytic mechanism

Received June 2, 2011; accepted July 29, 2011; published online August 13, 2011

Koh Ida[1,2], Masaya Suguro[3] and Haruo Suzuki[1,3,*]

[1]Department of Biosciences, School of Science, Kitasato University, Kitasato 1-15-1, Sagamihara, Kanagawa 252-0329; [2]RIKEN SPring-8 Center, Hyogo 679-5148 and [3]Division of Bioscience, Graduate School of Fundamental Life Science, Kitasato University, Kitasato 1-15-1, Sagamihara, Kanagawa 252-0329, Japan

*Haruo Suzuki, Department of Biosciences, School of Science, Kitasato University, Kitasato 1-15-1, Sagamihara, Kanagawa 252-0329, Japan. Tel: +81 42 741 5526, Fax: +81 42 741 5526, email: suzukih@kitasato-u.ac.jp

Atomic coordinates and structure factors have been deposited with the Protein Data Bank (accession code: 3AYI, 3AYJ and 3AYL).

The mature form of L-Phe oxidase of *Pseudomonas* sp. P-501 (PAOpt) catalyzes the oxygenative decarboxylation of L-Phe and the oxidative deamination of L-Met, and is highly specific for L-Phe. The crystal structures of PAOpt individually complexed with L-Phe and L-Met and the properties of the active site mutants were investigated to clarify the structural basis of the substrate and reaction specificities of the enzyme. The benzene ring of L-Phe is packed in six hydrophobic amino acid side chains versus the two hydrophobic side chains of L-amino acid oxidase (LAO, pdb code: 2jb2); the distance between the substrate Cα atom and water is shorter in the PAOpt-L-Met complex than in the PAOpt-L-Phe complex; and the mutation of substrate carboxylate-binding residues (Arg143 and Tyr536) causes the enzyme to oxidize L-Phe and decreases the charge-transfer band with L-Phe. These results suggest that (i) the higher substrate specificity of PAOpt relative to LAO is derived from the compact hydrophobic nature of the PAOpt active site and (ii) the reactivity of the PAOpt charge–transfer complex with water or oxygen determines whether the enzyme catalyzes oxidation or oxygenation, respectively.

Keywords: catalytic mechanism/crystal structure/enzyme specificity/flavoprotein/putative tryptophan monooxygenase.

Abbreviations: AB, *o*-aminobenzoate; DAO, D-amino acid oxidase; LAO, L-amino acid oxidase; PAM, phenylacetamide; PPA, 3-phenylpropionate; PPV, phenylpyruvate; PAO, L-phenylalanine oxidase from *Pseudomonas* sp. P-501; PAOpt, the activated form of proPAO; proPAO, non-catalytic pro-form of PAO; wt, wild-type.

L-amino acid oxidases (LAOs) are homodimeric flavoproteins containing a non-covalently bound FAD molecule as a cofactor in each subunit. These enzymes catalyse the oxidative deamination of L-amino acid substrates to convert them to their corresponding α-keto acids. This reaction includes production of ammonia, and hydrogen peroxide. LAOs are generally non-specific with regard to the amino acid side chain and accept most of the 20 proteinogenic L-amino acids as substrates (*1*–*3*). Some exceptions have been reported, such as L-phenylalanine oxidase from *Pseudomonas* (*4*), L-glutamate oxidases from *Streptomyces* (*5*, *6*) and LAO from *Lechevalieria aerocolonigenes* (*7*). Among these enzymes, L-Glu oxidases from *Streptomyces* (*5*, *6*) and LAO from *L. aerocolonigenes* ATCC 39243 (*7*) are highly specific for L-Glu and L-Trp, respectively.

L-Phe oxidase (deaminating and decarboxylating, EC 1.13.12.9: PAO) from *Pseudomona* sp. P-501 catalyses both oxidative deamination and oxygenative decarboxylation, depending on the substrate used (*4*, *8*). The enzyme has relatively high activity for L-Phe and L-Tyr, but relatively low activity for L-Met and L-Trp. Among these amino acids, L-Phe is mainly oxygenated and L-Met is mainly oxidized. PAO is expressed as a non-catalytic pro-enzyme (proPAO) that is activated by Pronase–trypsin treatment of proPAO to form the active enzyme (PAOpt) (*9*). Previously, we reported the crystal structures of proPAO, PAOpt and the PAOpt-o-aminobenzoate (AB) complex (*10*). Using these structures, we showed that the cofactor FAD is accessible by solvent through a funnel and that the funnel is occupied by the prosequence of proPAO. This explains the lack of catalytic activity exhibited by proPAO.

An enzyme similar to PAO was reported to be included in the gene sequences of *Ralstonia solanacearum* (*11*, *12*) and named putative tryptophan monooxygenase. Recently, the putative tryptophan monooxygenase gene from *R. solanacearum* was expressed and characterized to be PAO (*13*). *Ralstonia solanacearum* is considered to be one of the most important plant pathogenic bacteria, causing wilt, and leading to plant death [see reference (*14*) for review and references therein].

Studies on the mechanisms and structures of flavoprotein amine-oxidizing enzymes have been reviewed (*15*–*20*). The flavin-dependent oxidase reaction can be divided into two separate reactions, a reductive half-reaction and an oxidative half-reaction. In the

reductive half-reaction, a flavin cofactor oxidizes the substrate, and the reduced cofactor is subsequently oxidized by molecular oxygen in the oxidative half-reaction. Mechanistic studies have focused on substrate oxidation, and several mechanisms were proposed, including 'carbanion', 'ionic' and 'hydride transfer' mechanisms. With regard to L-amino acid oxidase, recent detailed structural studies on the enzyme revealed that hydride transfer is the mechanism of substrate dehydrogenation (*21*, *22*). In contrast to the reductive half-reaction, the chemical basis of oxygen reactivities remains undetermined (*19*). However, recent studies on flavoprotein oxidases and oxygenases have identified the oxygen trajectory and the oxygen-binding site in the enzyme and have also identified the flavin C(4a)-hydroperoxy adduct intermediate in the oxidative half-reaction (*19*, *23*–*29*).

On the basis of spectral and kinetic studies, the reaction of PAO with β-thienylalanine (oxygenase substrate) and L-Met (oxidase substrate) as substrates is explained by the same kinetic scheme (*30*). The oxidized form of enzyme binds with substrate to form the enzyme-substrate complex, which changes to the purple intermediate, a charge–transfer complex consisting of the reduced enzyme and an imino acid derived from a substrate, and the charge–transfer complex reacts with molecular oxygen to reform the oxidized form of enzyme and to produce the reaction products (*30*, *31*) (Scheme 1). To elucidate the reaction mechanism of the enzyme at the atomic level, crystal structures of PAOpt individually complexed with 3-phenylpropionate (PPA), L-Phe and L-Met were constructed at 1.0–1.25 Å resolution, and a site-directed mutagenesis study of active site residues was performed. Combining the structural and mutagenesis studies has allowed us to explain its high substrate specificity and to propose a reaction mechanism of PAO in relation to its oxidase and oxygenase reactions.

Materials and Methods

Enzyme purification and crystallization

The proPAO protein was expressed in *Escherichia coli* and purified as described previously. PAOpt was obtained by treatment of proPAO with Pronase and trypsin (*9*). The purity of the enzymes was confirmed by SDS–PAGE. The amino acid residue numbering scheme of PAO is the same as that of the proPAO polypeptide. A solution of purified protein in 10 mM Tris–HCl (pH 8.0) was concentrated to 10 mg/ml in an Amicon Ultra concentrator (Millipore) at 277 K. Crystallization was performed by the vapour diffusion method. The enzyme solution (PAOpt) was mixed with an equal volume of a reservoir solution consisting of 0.1 M HEPES (pH 7.5) and 1.0 M ammonium sulphate. The crystal has a shape similar to that of a gold ingot (Supplementary Fig. S1) and has a size of ~1 mm.

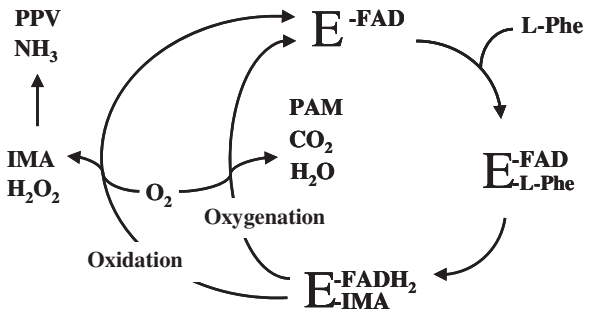

Scheme 1 Reaction mechanism of *Pseudomonas* L-Phe oxidase (deaminating and decarboxylating). The enzyme contains two FAD cofactors, but the scheme is expressed per FAD. PAM, PPV and IMA represent phenylacetamide, phenylpyruvate and imino acid, respectively.

Data collection, structure solution and refinement

Diffraction data sets were collected on NW12 at the PF-AR (Tsukuba, Japan) and BL44B2 at the SPring-8 Centre (Hyogo, Japan). The complexes of PAOpt with PPA, L-Phe and L-Met were prepared by soaking the crystals in the crystallization buffer containing 30% glycerol and these ligands. The ligand concentration was 10 mM, and the diffraction data were collected after the yellow colour of the crystal was changed to purple with L-Phe, pale yellow with L-Met and decreased slightly with PPA. The temperature of the data collection was 100 K. In all cases, the initial model of the structures was derived from the proPAO structure (pdb id: 2yr4) (*10*). The refinement resolution was 1.10 Å for the PAOpt-L-Phe complex, 1.25 Å for the PAOpt-L-Met complex and 1.25 Å for the PAOpt-PPA complex. These structural refinements were carried out by REFMAC5 (*32*) and SHELX (*33*) with an anisotropic temperature factor. The initial ligand models were the structures of free L-Phe and L-Met, and refined using REFMAC5 with default parameters. The quality of the diffraction data statistics and the refinement statistics are given in Table I. The graphic images of these structures were generated using the PyMOL program (*34*). Chimera software was used to match the structures (*35*). Channels of the enzyme were identified by the CAVER program (PyMOL plugin, *36*, *37*).

Site-directed mutagenesis

Site-directed mutagenesis of residues Arg143 and Tyr536 of proPAO was carried out using a QuikChange XL site-directed mutagenesis kit according to the manufacturer's recommendations (Stratagene). The desired mutation was introduced on the wt proPAO gene in the plasmid, $pPAO_{+15}$ (*9*). Hereafter, the term 'wt' (wild-type protein) refers to the recombinant (protein) without mutations. The mutagenic change was confirmed by sequencing the mutant plasmid gene. Sequencing was performed by the Genomic Research Department of Shimadzu-Biotech. The proPAO mutants were expressed in *E. coli* BL21(DE3) and purified. The PAOpt mutants R143K, R143A, Y536F and Y536A were activated from their respective proPAO mutants and purified as described previously (*9*).

Assay of enzyme activity

The rate of overall reaction was estimated by measuring the consumption of oxygen dissolved in the reaction mixture with a Clark-type oxygen electrode (Strathkelvin Instruments). The reaction mixture contained various concentrations of substrate in 20 mM potassium phosphate (pH 7.0) at 25°C. The rate (v) was expressed as the molar concentration of oxygen consumed per second per molar concentration of the enzyme-bound FAD. The concentration of enzyme was expressed according to the FAD content, which was determined by measuring the absorbance at 450 nm, using the molar extinction coefficient of 11.3 $mM^{-1}cm^{-1}$ at 450 nm. The apparent kinetic parameters were determined from the rates obtained with various concentrations of L-Phe or L-Met.

Spectroscopy

Absorption spectra were measured at 25°C using a double beam spectrophotometer, type Ubest-50, from Japan Spectroscopic. Buffer used was 20 mM potassium phosphate (pH 7.0).

Product analysis

The reaction mixture (3.1 ml) containing an indicated concentration of L-Phe and enzyme in potassium phosphate buffer (pH 7.0) was incubated for an indicated time in the reaction vessel equipped with a Clark-type oxygen electrode. When approximately half of the oxygen in the mixture was consumed, 380 µl of the mixture was removed and mixed with 20 µl of 10 M $HClO_4$ to stop the reaction.

Table I. Data collection, refinement and model statistics.

	PPA	Phe	Met
Data collection			
Beamline	PF-AR(NW12)	SPring-8 (BL44B2)	PF-AR (NW12)
Wavelength (Å)	1.0000	0.80000	1.00000
Space group	$P2_12_12_1$	$P2_12_12_1$	$P2_12_12_1$
Unit cell (Å)	$a=101.29$, $b=112.69$, $c=136.54$	$a=100.99$, $b=112.94$, $c=136.46$	$a=101.27$, $b=112.84$, $c=136.49$
Resolution range[a] (Å)	37.56–1.25 (1.32–1.25)	29.20–1.10 (1.16–1.10)	36.27–1.25 (1.32–1.25)
Measured reflections	1,962,049	3,277,203	2,084,318
Unique reflections	415,716	615,937	415,723
Redundancy	4.7 (4.1)	5.7 (5.7)	5.0 (4.9)
Completeness (%)	97.3 (87.0)	98.6 (97.1)	97.4 (98.4)
R_{merge}[b] (%)	6.9 (32.9)	4.3 (39.8)	7.7 (34.7)
I/σ	4.6	9.1	4.7
Refinement			
Resolution range[a] (Å)	37.56–1.25 (1.32–1.25)	29.20–1.10 (1.16–1.10)	36.27–1.25 (1.32–1.25)
R_{work} (%)	10.3	11.1	9.9
R_{free} (%)	13.1	13.0	12.8
Model Statistics			
Rmsds			
Bond length (Å)	0.030	0.025	0.026
Bond angles (deg)	2.442	2.154	2.298
Average B-factor (Å^2)			
All chains	11.805	11.816	10.515
FAD	8.667	8.761	6.982
Ramachandran plot(%)			
Allowed region	98.0	98.0	97.8
Generously allowed region	1.8	2.0	2.1
Disallowed region	0.2	0.0	0.1

[a]Values in parentheses correspond to the reflections observed in the highest resolution shell.
[b]$R_{merge}=\sum_{hkl}\sum_i|I_{hkl,i}-\langle I_{hkl}\rangle|/\sum_{hkl}\sum_i I_{hkl,i}$, where I is the observed intensity and $\langle I\rangle$is the averaged intensity for multiple measurements.

The mixture was centrifuged to remove the precipitates, and the supernatant was analysed by HPLC using a TSKgel SUPER-ODS column (Tosoh, 4.6 mm × 10 cm). Products were eluted at a flow rate of 1 ml/min with 90 mM potassium phosphate (pH 7.0) containing 10% methanol.

Results

Active site structures of PAOpt-ligand complex

The structures of PAOpt in complex with various ligands were analysed by the X-ray crystallography. L-Phe and L-Met were used as an amino acid ligand. PPA was also selected as a ligand, since it is the analog of Phe and a competitive inhibitor of L-Phe (K_i: $13.9\pm0.2\,\mu M$). When the PAOpt crystal was soaked in the crystallization buffer containing L-Phe, the crystal changed yellow to purple (Supplementary Fig. S1), confirming that the enzyme in the crystal forms a charge-transfer complex as observed in the solution. However, we observed that the crystal of the purple intermediate lost its colour at the region that was exposed to the X-ray. We tested the stability of the purple intermediate against X-ray exposure using a microspectrophotometer, which is coupled to the BL44B2 beam line at SPring-8, and found that the crystal remained purple with an X-ray exposure of 2×10^{14} photons (data not shown). We constructed the present structural model from X-ray diffraction data obtained with X-ray exposure of 3.6×10^{14} photons, but the crystal lost its colour after data collection. In the case of L-Met, the enzyme changed from yellow to pale yellow after soaking the PAOpt crystal with a solution of L-Met. This result supports the interpretation that L-Met has a weak charge–transfer band (*30*).

The superposition of the Cα atoms of the PAOpt structures in complex with PPA, L-Phe and L-Met on those of the PAOpt structure (pdb code, 2yr5, *10*) results in RMSD values of 0.13, 0.14 and 0.15 Å, respectively. This suggests that the overall structure of PAOpt does not change significantly upon binding of ligands. Therefore, we analysed the ligand-binding region in the structures. Figure 1A shows the structure of the binding region of PPA (the structures of the flavin ring, PPA, and the reaction products are shown in Fig. 2). PPA is bound to the *re*-side of the flavin ring of FAD and the benzene ring of PPA is surrounded by hydrophobic residues F316, L319, L330, Y335, W538, F617, L619 and W660. The hydrophobic environment of the binding site may explain the high affinity of PPA for the enzyme. Figure 1B and C show the structures of the binding site of L-Phe and L-Met in PAOpt, respectively. The amino acid residues in the vicinity of the bound amino acids are the same as those located in the vicinity of PPA. Among these hydrophobic side chains, there are two H-π interactions in the PAOpt-L-Phe complex. W660 interacts with H-N, and F617 interacts with H-Cβ (Fig. 1D). In our previous report (*10*), we proposed that the side chains of F617 and W660 form an 'aromatic cage' observed in monoamine oxidase (*38*) and the side chain of L-Phe is packed in the cage. The 3D structure of the PAOpt-L-Phe complex supports this proposal (Fig. 1B). It was found that the electron density map of the side chain of L-Met is not well defined (Fig. 1C). The hydrophobic residues (F316, L319 and L619) are

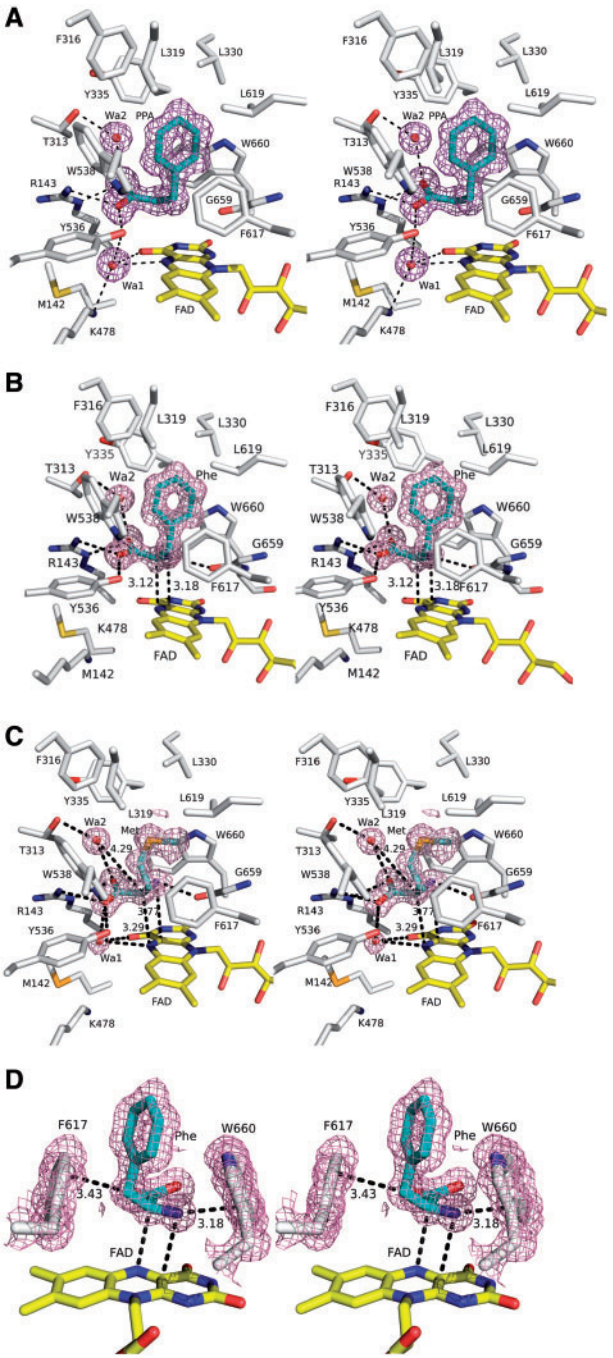

Fig. 1 Stereo views of the active site of PAOpt-PPA (A), PAOpt-L-Phe (B), and PAOpt-L-Met (C) complexes, and of the aromatic cage in the PAOpt-L-Phe complex (D). The carbon atoms of the ligands are shown in cyan. The water molecule is shown by a red CPK model. The O and N atoms are coloured red and blue, respectively. The 2Fo-Fc electron density map is contoured at 1 σ around the bound ligands, and the water molecules are hydrogen-bonded to the ligands.

~4 Å apart from the Cε atom of L-Phe and ~5 Å apart from the Sδ atom of L-Met (Fig. 5B). These observations suggest that the side chain of L-Met is much easier to move than that of L-Phe.

Structures of substrates in the PAOpt active site

The configuration of the bound substrate was analysed by measuring the bond angles around the Cα atom,

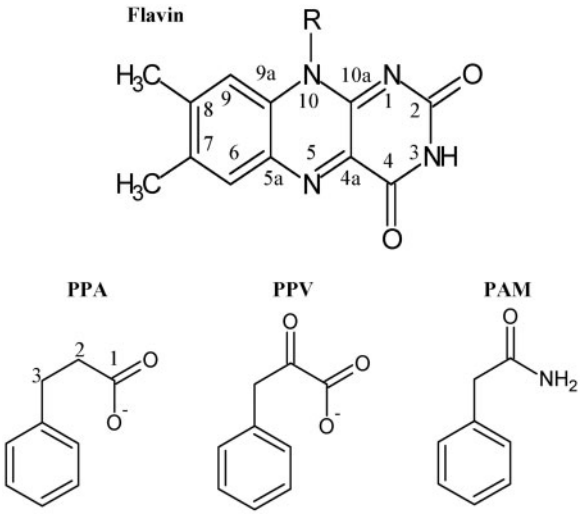

Fig. 2 Structures of flavin ring, PPA, PPV and PAM.

since we considered that it is better to measure the bond angle around the Cα atom to estimate the extent of sp^2 and sp^3 configurations. The sum of the angles will be 360° (=120° × 3) for the ideal planar sp^2 configuration, and 328.5° (=109.5° × 3) for the ideal tetrahedral sp^3 configuration. In the structure of the PAOpt-L-Phe and PAOpt-L-Met complexes, the angles around the Cα atom do not correspond to those of an ideal tetrahedron (L-Phe: ∠NCαC = 111.4°, ∠NCαCβ = 115.1°, ∠CCαCβ = 115.0°; L-Met: ∠NCαC = 111.3°, ∠NCαCβ = 112.1°, ∠CCαCβ = 113.2°) and the sum of the angles were calculated to be 341.5° and 336.6°, respectively. These values mean that the PAOpt-L-Phe and PAOpt-L-Met complexes contain ~38% and ~8% of imino acid, respectively. This is equivalent to containing ~62% and ~92% of the respective L-amino acids. These values are probably overestimated, since we modelled the ligand structure by REFMAC5 with default parameters as described in 'Materials and Methods' section.

The bond angles around the Cα atom of the bound L-Phe show the tetrahedral sp^3 configuration in the LAO-L-Phe complex (pdb code: 2iid for crLAO) (*21*). The authors suggested that when the crystal is soaked with L-Phe, the product imino acid is released from the enzyme, and another L-Phe molecule binds to the site before oxidation of the reduced flavin occurs. As for the yDAO-D-Ala structure (pdb code: 1c0p) (*39*), the authors calculated the occupancy of D-Ala and iminopyruvate to be ≥2 : 1, by comparing the Cα–N bond length of the bound D-Ala with the corresponding length of the free D-Ala (1.47 Å) and with the carbonyl bond (1.21 Å). We collected the diffraction data for the crystal of the purple intermediate. The crystal was cooled during the data collection by flushing with liquid nitrogen gas. It is therefore impossible for another L-Phe to bind to the active site of enzyme as proposed for LAOs (*21*, *22*). It is conceivable that the X-ray irradiation induces reduction of the imino acid to re-form the original substrate, although we

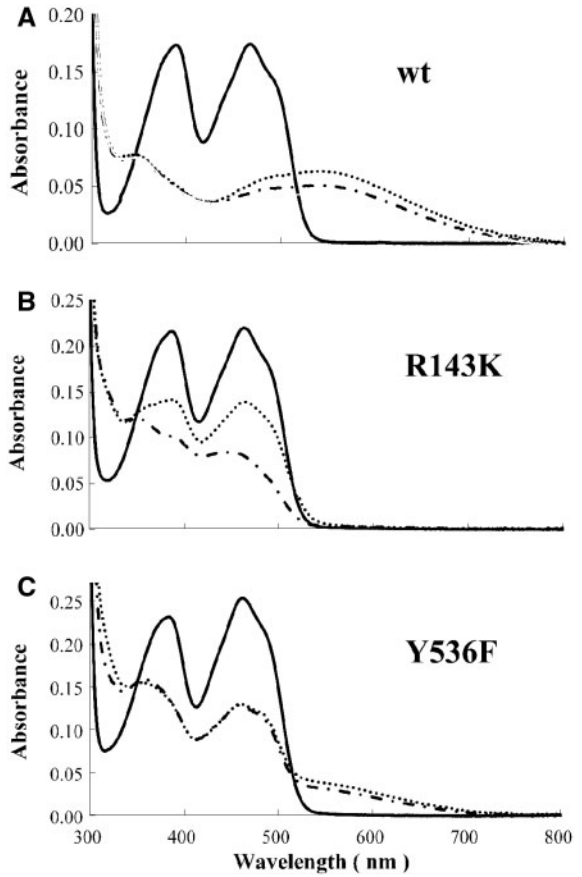

Fig. 3 Spectral change in the PAOpt mutant by the addition of 2 mM L-Phe under aerobic conditions. The final concentration of enzyme was 15.4 μM for wt (A), 19.4 μM for R143K (B) and 22.2 μM for Y536F (C) mutant enzymes. To the enzyme solution in 20 mM potassium phosphate (pH 7.0), L-Phe was added at the final concentration of 1 mM, and the whole was mixed and the spectral changes were measured. The temperature was 25°C. Solid line, before addition of L-Phe; dash line, just after addition of L-Phe; dash dot line, 30 min after addition of L-Phe.

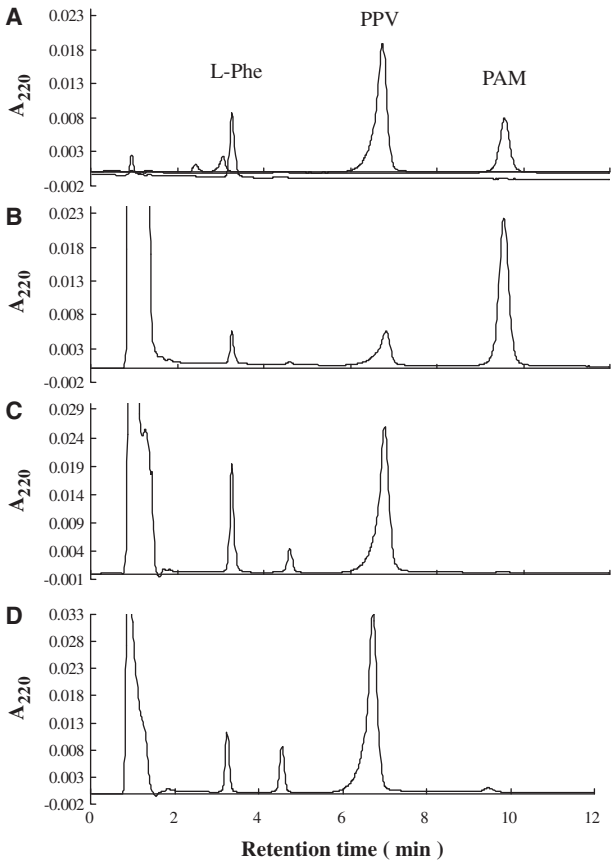

Fig. 4 HPLC analysis of products formed after incubation of L-Phe with the wt and mutant enzymes. After incubation of L-Phe with the wt (B), R143K (C) and Y536F (D) mutant enzymes, reactions were stopped by additing $HClO_4$ at a final concentration of 0.5 M as described in 'Materials and Methods' section. (A) standard, L-Phe; PPV, phenylpyruvate; PAM, phenylacetamide.

do not have any evidence that irradiation affects the imino acid.

Structures of isoalloxazine ring in the PAOpt ligand complexes

The structure of isoalloxazine ring was reported to change with its redox state of the flavin models and yDAO (*39*, *40*). Based on the structures of PAOpt in complex with and without various ligands, the N(5)–C(4a) lengths of the flavin ring in PAOpt, and the PAOpt-PPA and PAOpt-AB (pdb code: 2yr6) complexes, which contain the oxidized flavins, were found to be 1.39, 1.36 and 1.37 Å, respectively. The lengths of the flavin ring in the PAOpt structure in complex with L-Phe and L-Met, which contain the reduced flavins, were found to be 1.37 Å and 1.40 Å, respectively. These results suggest that the N(5)–C(4a) length does not change with the redox state of the PAOpt flavin ring. The oxidized isoalloxazine ring is more planar than the reduced ring in the model study (*40*). Therefore, we determined the dihedral angle around the N(5)–N(10) axis of the isoalloxazine ring atoms C(4), N(5), N(10) and C(6) in the PAOpt structures determined in the present and previous studies. The angles show that the flavin ring is bent ~6° in the PAOpt-PPA and PAOpt-L-Phe complexes, and ~15° in PAOpt, and the PAOpt-AB and PAOpt-L-Met complexes. From these results, there are no direct correlation between the structure of the flavin ring and its redox state, rather the structure of the flavin ring changes with ligand used.

Site-directed mutagenesis of Arg143 and Tyr536

Three-dimensional structures of PAOpt showed that Arg143 interacts with the carboxylate group of substrates and of PPA (Fig. 1). Sobrado and Fitzpatrick (*41*, *42*) reported that for tryptophan 2-monooxygenase, the site-directed mutation of the active site residues, Arg98 and Tyr413 alters the activity of the enzyme so that it oxidizes the substrate L-Trp. These residues interact with the carboxylate group of L-Trp. The corresponding residues are Arg143 and Tyr536 in PAO. Therefore, the site-directed mutants of these residues were prepared and characterized as described in 'Materials and Methods' section. The R143A and Y536A mutant enzymes were found to have no activity while the R143K and Y536F mutants were found to

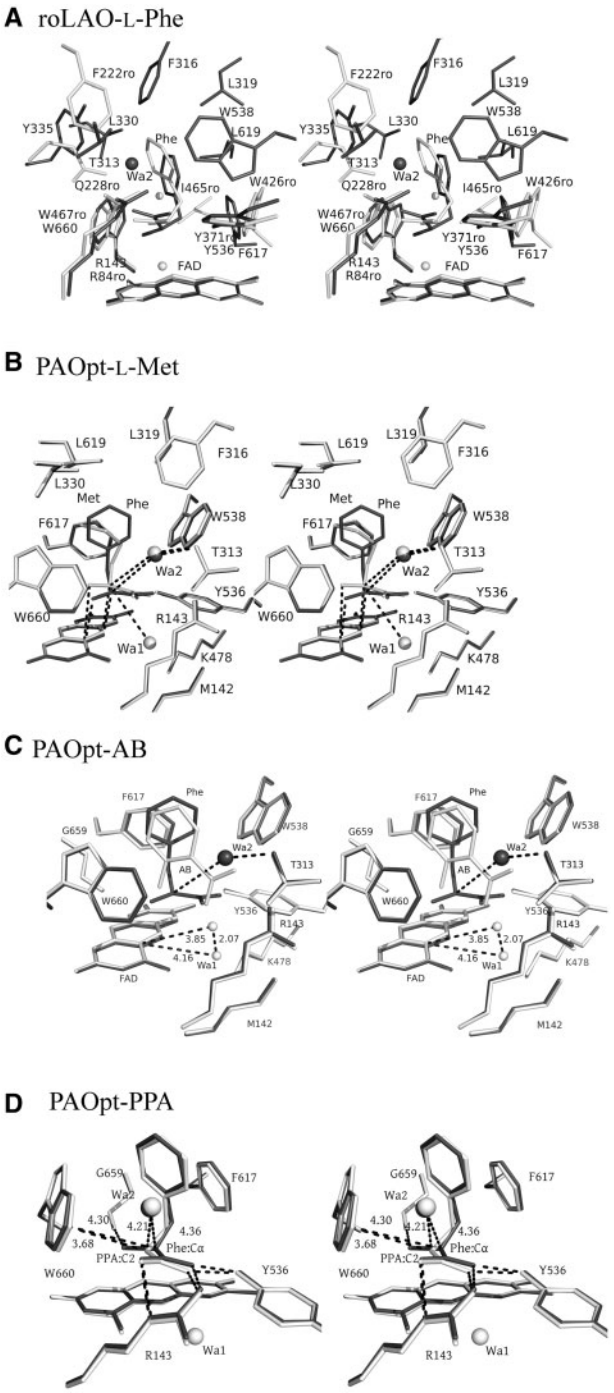

Fig. 5 Stereo view of the active site of the PAOpt-L-Phe complex superimposed on the active site of the roLAO-L-Phe (A), PAOpt-L-Met (B), PAOpt-AB (C) and PAOpt-PPA (D) complexes. The carbon atom of the PAOpt-L-Phe complex was coloured black and that of the other complexes were coloured white. The amino acid residue of roLAO (pdb code: 2jb2) was shown by adding the subscript 'ro'.

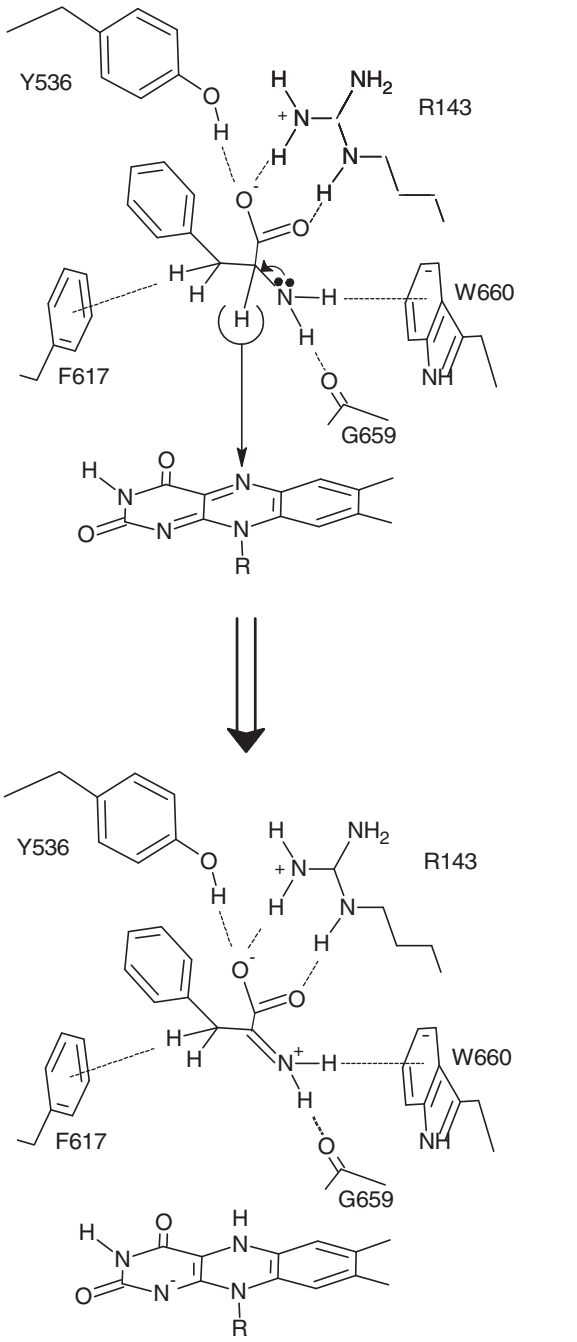

Scheme 2 A proposed mechanism of the substrate dehydrogenation.

have ~400- and ~17-fold lower activity than the wt enzyme, respectively (Supplementary Table S2).

Upon addition of L-Phe to the R143K and Y536F mutants, a charge-transfer band becomes weakly observable in the case of the Y536F mutant, but not for the R143K mutant (Fig. 3). This indicates that the interaction of the substrate carboxylate group with the guanidinium group of Arg143 provides fine orientation of the imino acid with respect to the reduced isoalloxazine ring. To further assess the effect of the mutation on the enzyme, the reaction products of these mutants were analysed. Figure 4 shows that the wt PAOpt produces higher amounts of phenylacetamide (PAM) than phenylpyruvate (PPV) as expected, but PAM was not produced by the R143K and Y536F mutants. There is an unknown peak at ~4.5 min, which has been assigned as phenylacetate. We expect that this compound is produced by oxidation of PPV with H_2O_2, because the peak also appears upon mixing of PPV with H_2O_2 in the reaction mixture (data not

shown). The Y536F mutant was found to display a weak charge-transfer band similar to that observed with the wt type enzyme mixed with L-Met (*30*). These data lead us to conclude that the enzyme activity is altered to oxidize L-Phe as a result of the mutations.

Discussion

Substrate specificity

PAOpt has relatively high activity with respect to L-Phe and L-Tyr, and relatively low activity with respect to L-Met and L-Trp (Supplementary Table S1). This suggests that the benzene ring of the side chain has an important influence on the activity. As described in the Results, the active site pocket is composed of eight hydrophobic amino acid side chains. The benzene ring of L-Phe is well fitted in the pocket. However, the side chain of L-Met does not fit well within the active site pocket and is more mobile than L-Phe (Fig. 5B), explaining the lower activity with L-Met as compared with L-Phe. The relatively lower activity with respect to L-Trp (~20% of the activity for L-Phe, Supplementary Table S1) might be due to the bulky side chain of L-Trp, which does not fit well within the pocket.

To elucidate why LAO from *Rhodococcus opacus* (roLAO, pdb code: 2bj2, *22*), in contrast to PAO, is non-specific with respect to the amino acid side chains, the structure of the roLAO-L-Phe complex was superimposed on that of the PAOpt-L-Phe complex (Fig. 5A). The Cβ and N atoms of L-Phe in both the PAOpt complex with L-Phe and the roLAO complex with L-Phe interact with the aromatic cage residues via H-π bonds, but the bond lengths in roLAO are longer than those of PAOpt. In addition to the cage residues, the benzene ring of L-Phe in PAOpt is surrounded by six hydrophobic residues, F316, L319, L330, Y335, W538 and L619, but in roLAO, the benzene ring of L-Phe appears to interact weakly with two hydrophobic residues, F222 and I465. Therefore, the benzene ring of L-Phe is more closely packed in the active site of PAOpt than in the active site of roLAO. Thus, the active site pocket of roLAO can individually accommodate the 20 proteinogenic amino acids (*1–3*). Moreover, the trajectory of the substrate is gated by the hydrophobic residues in the channel in PAOpt, but substrate freely diffuses through the channel in roLAO. These facts explain the observation that PAOpt is highly specific while roLAO is unspecific with respect to the side chains of the amino acids.

Dehydrogenation of substrate

In the active site of PAOpt, the positive charge of Arg 143 is neutralized by binding with the carboxylate ion of substrate. To accommodate the hydrophobic nature of the active site, p*K*a of the substrate amino group must be decreased to form the unprotonated form of amino acid at neutral pH. The shift of p*K*a value (Δp*K*a = 2 ~ 3.5) of substrate amines to the acid pH was reported for trimethylamine dehydrogenase (*43*), monomeric sarcosine oxidase (*44*) and monoamine oxidase (*45*). Therefore, the unprotonated form of amino acid substrate is assumed to be the reactive substrate in the present study. As described in 'Results' section, the isoalloxazine ring in the PAOpt substrate complex is in the reduced form, and the bound substrate is in the form of a mixture of the substrate and its corresponding imino acid. The bound substrate is ~60% of the amino form in the PAOpt-L-Phe complex, and ~90% of the amino form in the PAOpt-L-Met complex. The conformation of the isoalloxazine ring does not change greatly with changes in the redox state of the ring. Therefore, we discuss the reaction mechanism by assuming that the amino acid substrate is interacting with the oxidized flavin in the PAOpt-L-Phe and PAOpt-L-Met complexes (Fig. 1B and C). From the structural studies of yDAO (*39*) and LAOs (*21*, *22*), it has been proposed that 'hydride transfer' is included in the mechanism of dehydrogenation on the basis of the following facts. The Cα-H of the bound amino acid points toward the flavin N(5) atom and no functional group is present in the active site that could act as an acid-base catalyst for Cα-H bond cleavage in the substrate. The distance between the N(5) atom of the isoalloxazine ring and the Cα atom of the bound amino acid in the PAOpt complex with L-Phe and L-Met were 3.12 and 3.29 Å, respectively. These distances are short enough to allow direct transfer of hydride to the flavin N(5) atom (Fig. 1B and C). Moreover, there is no functional group capable of acting as an acid-base catalyst in the active site. These facts lead to the proposal that PAOpt dehydrogenates L-Phe and L-Met using the hydride transfer mechanism (Scheme 2).

Oxidative deamination and oxygenative decarboxylation

Kinetic studies (*30*) suggest the reactivity of the charge–transfer complex with molecular oxygen determines the reaction specificity (Scheme 1). Therefore, we consider the protein structure around the ligands, and the distances between the isoalloxazine ring, the water molecule and each of the ligands in the PAOpt-L-Phe and PAOpt-L-Met complexes. When the imino acid leaves the reduced FAD moiety, it reacts with water to form the corresponding keto acid and ammonia. There are two water molecules at the active site (Fig. 1A, C; Wa1 and Wa2 in Fig. 5B). One is located near the side chain of K478 (Wa1), and the other is near the T313 side chain (Wa2). There is no electron density near the K478 side chain in the PAOpt-L-Phe complex, but there is electron density identified as a water molecule in the structure of the PAOpt-L-Met complex (compare Fig. 1B with C). In the previous work, we proposed on the basis of the PAOpt-AB structure (pdb code: 2yr6) that the oxygen molecule binds to the Wa1 site (Fig. 5C). Therefore, we suggest that molecular oxygen resides in the vicinity of Wa1 and the candidate water molecule, which reacts with the imino acid, is Wa2 (Fig. 5B). The distance between the Cα atom and Wa2 in the PAOpt-L-Met complex (4.29 Å) is shorter than that of the PAOpt-L-Phe complex (4.36 Å) (Fig. 5B). From these results, we propose that the distance between the Cα atom of amino acid substrates and Wa2 is relatively short and that the imino intermediate reacts with Wa2 to initiate the oxidative deamination reaction. The results obtained with the mutants support the idea. It is conceivable that the

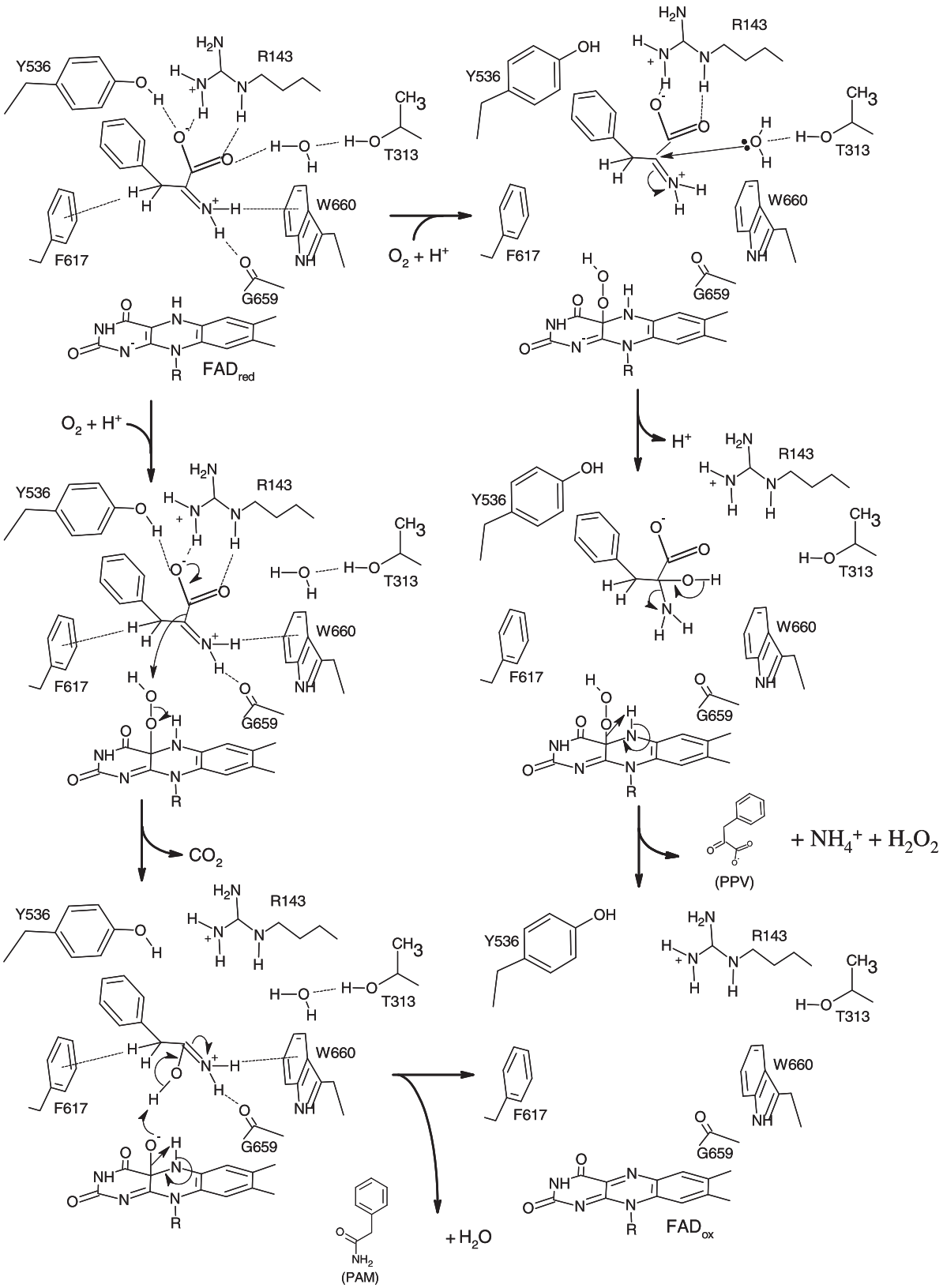

Scheme 3 A catalytic mechanism of t oxidative deamination and oxygenative decarboxylation of L-Phe.

proper positioning of the Cα atom in the PAOpt-L-Phe complex is determined by the side chains of R143, Y536, the main chain O atom of G659, and the aromatic cage (Fig. 1D). PPA does not have an amino group, and does not interact with the main chain O atom of G659. As a result, the distance from water molecule (Wa2) to the C2 atom (4.21 Å) becomes shorter than the distance from Wa2 to the Cα atom

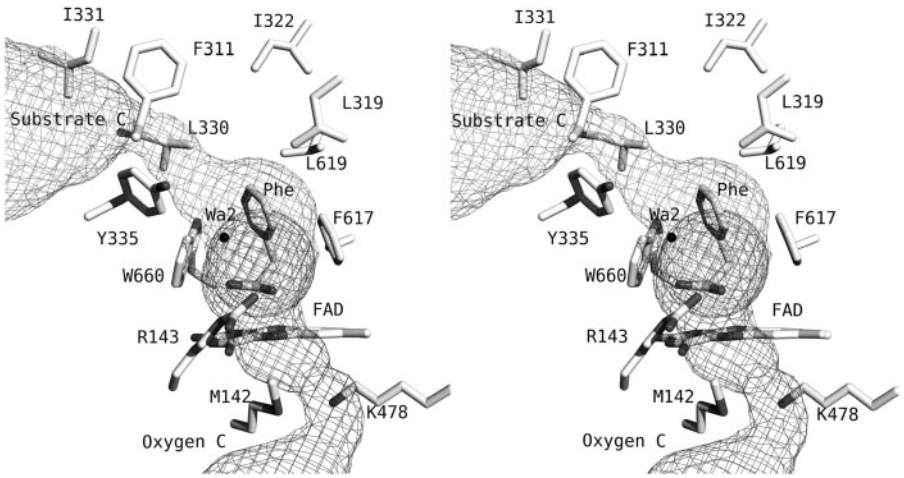

Fig. 6 Substrate and oxygen channels at the active sites of PAOpt. The substrate and oxygen channels have been proposed previously (*10*), and are represented as Substrate C and Oxygen C, respectively. The tunnels were identified for the structure of the PAOpt-L-Phe complex.

of L-Phe (4.36 Å, Fig. 5D). Although the active site structures of the R143K and Y536F mutants in complex with L-Phe are not known, it is clear that one of the three interactions of the carboxylate group of L-Phe with the active site residues is lost as a result of the mutation. Therefore, the distance of the Cα atom of L-Phe from Wa2 might be shortened. The idea is supported by the fact that no or weak charge-transfer band were observed with the mutants (Fig. 3B and C), suggesting a weak interaction between the imino group and the flavin ring. This weak interaction increases the distance from the flavin ring to the imino group, thus shortening the distance from the Cα atom of the imino intermediate to Wa2.

The flavin C(4a)-hydroperoxide adduct has been observed in oxygenases during the oxidative half-reaction of the reduced flavin with molecular oxygen (*26*, *29*, *46*, *47*). As for flavoprotein oxidases, Sucharitakul *et al*. (*28*) observed a typical C(4a)-hydroperoxyflavin spectrum with an absorption maximum of about 400 nm during the oxidative half-reaction of pyranose 2-oxidase of *Trametes multicolor*. Mattevi (*19*) reviewed the oxygen reactivity of flavoprotein oxidases, and showed that there are properly positioned positive charges in their active sites. We previously suggested that oxygen-binding at the PAOpt active site occurs near the Lys478 and Met142 residues (Fig. 5C) (*10*). Fig. 6 shows the results of the tunnel analysis of PAOpt-L-Phe complex by CAVER (*36*, *37*). There is a sufficient space to accommodate an oxygen molecule at the region of the channel, which makes contact with N(5) of the flavin ring, the methyl group of M142, and the ε amino group of K478 (Fig. 6). These interactions contribute to the process of binding of the oxygen molecule (*19*). Therefore we wish to propose the reaction mechanism set forth in Scheme 3 to explain the oxidative deamination and oxygenative decarboxylation, including the C(4a)-hydroperoxyflavin adduct. We believe that this is an appropriate mechanism although we did not detect the adduct during the oxidative half-reaction of the reduced PAOpt with molecular oxygen.

Supplementary Data

Supplementary Data are available at *JB* Online.

Acknowledgements

The authors thank Drs T. Hikima, G. Ueno and M. Yamamoto (RIKEN SPring-8 Centre, Division of Synchrotron Radiation Instrumentation) for assistance with the X-ray data collection. This work was performed with approval by the Photon Factory Program Advisory Committee (proposal No, 2004G372 and 2006G368). K.I. was supported by Kitasato University Research Grant for Young Researchers. The authors wish to thank Prof. Y. Nishina of the Faculty of Life Sciences, Kumamoto University, for critical reading of the manuscript.

Conflict of interest
None declared.

References

1. Bender, A.E. and Krebs, H.A. (1949) The oxidation of various synthetic α-amino-acids by mammalian D-amino acid oxidase, L-amino-acid oxidase of cobra venom and the L- and D-amino acid oxidases of *Neurospora* crassa. *Biochem. J.* **46**, 210–219
2. Thayer, P.S. and Horowitz, H. (1951) The L-amino acid oxidase of Neurospora. *J. Biol. Chem.* **192**, 755–767
3. Kotaka, S. (1963) The L-amino acid oxidase from silkworm eggs (*Bombyx mori* L.). *J. Gen. Physiol.* **46**, 1087–1094
4. Koyama, H. (1982) Purification and characterization of a novel L-phenylalanine oxidase (deaminating and decarboxylating) from *Pseudomonas* sp. P-501. *J. Biochem.* **92**, 1235–1240
5. Kamei, T., Asano, K., Kondo, H., Matsuzaki, M., and Nakamura, S. (1983) L-Glutamate oxidase from *Streptomyces violascens*. II. Properties. *Chem. Pharm. Bull.* **31**, 3609–3616
6. Böhmer, A., Müller, A., Passarge, M., Liebs, P., Honeck, H., and Müller, H.-G. (1989) A novel L-glutamate oxidase from *Streptomyces endus*. Purification and properties. *Eur. J. Biochem.* **182**, 327–332
7. Nishizawa, T., Aldrich, C.C., and Sherman, D.H. (2005) Molecular analysis of the rebeccamycin L-amino acid

oxidase from *Lechevalieria aerocolonigenes* ATCC 39243. *J. Bacteriol.* **187**, 2084–2092

8. Koyama, H. (1984) Oxidation and oxygenation of L-amino acids catalyzed by a L-phenylalanine oxidase (deaminating and decarboxylating) from *Pseudomonas* sp. P-501. *J. Biochem.* **96**, 421–427
9. Suzuki, H., Higashi, Y., Asano, M., Suguro, M., Kigawa, M., Maeda, M., Katayama, S., Mukouyama, E.B., and Uchiyama, K. (2004) Sequencing and expression of the L-phenylalanine oxidase gene from *Pseudomonas* sp. P-501. Proteolytic activation of the proenzyme. *J. Biochem.* **136**, 617–627
10. Ida, K., Kurabayashi, M., Suguro, M., Hiruma, Y., Hikima, T., Yamomoto, M., and Suzuki, H. (2008) Structural basis of proteolytic activation of L-phenylalanine oxidase from *Pseudomonas* sp. P-501. *J. Biol. Chem.* **283**, 16584–16590
11. Salanoubat, M., Genin, S., Artiguenave, F., Gouzy, J., Mangenot, S., Arlat, M., Billault, A., Brottier, P., Camus, J.C., Cattolico, L., Chandler, M., Choisne, N., Claudel-Renard, C., Cunnac, S., Demange, N., Gaspin, C., Lavie, M., Moisan, A., Robert, C., Saurin, W., Schiex, T., Siguier, P., Thébault, P., Whalen, M., Wincker, P., Levy, M., Weissenbach, J., and Boucher, C.A. (2002) Genome sequence of the plant pathogen *Ralstonia solanacearum*. *Nature* **415**, 497–502
12. Gabriel, D.W., Allen, C., Schell, M., Denny, T.P., Greenberg, J.T., Duan, Y.P., Flores-Cruz, Z., Huang, M., Clifford, J.Q., Presting, G., González, E.T., Reddy, J., Elphinstone, J., Swanson, J., Yao, J., Mulholland, V., Liu, L., Farmerie, W., Patnaikuni, M., Balogh, B., Norman, D., Alvarez, A., Castillo, J.A., Jones, J., Saddler, G., Walunas, T., Zhukov, A., and Mikhailova, N. (2006) Identification of open reading frames unique to a select agent: *Ralstonia solanacearum* Race 3 Biovar 2. *Mol. Plant-Microbe Interact.* **19**, 69–79
13. Kurosawa, N., Hirata, T., and Suzuki, H. (2009) Characterization of putative tryptophan monooxygenase from *Ralstonia solanasearum*. *J. Biochem.* **146**, 23–32
14. Genin, S. and Boucher, C. (2002) *Ralstonia solanacerum*: secrets of a major pathogen unveiled by analysis of its genome. *Mol. Plant Pathol.* **3**, 111–118
15. Miura, R. and Miyake, Y. (1988) The reaction mechanism of D-amino acid oxidase: concerted or not concerted? *Bioorrg. Chem.* **16**, 97–110
16. Binda, C., Mattevi, A., and Edmondson, D.E. (2002) Structure-function relationships in flavoenzyme-dependent amine oxidations. A comparison of polyamine oxidase and monoamine oxidase. *J. Biol. Chem.* **277**, 23973–23976
17. Fitzpatrick, P.F. (2004) Carbanion versus hydride transfer mechanisms in flavoprotein-catalyzed dehydrogenations. *Bioorg. Chem.* **32**, 125–139
18. Scrutton, N.J. (2004) Chemical aspects of amine oxidation by flavoprotein enzymes. *Nat. Prod. Rep.* **21**, 722–730
19. Mattevi, A. (2006) To be or not to be an oxidase: challenging the oxygen reactivity of flavoenzymes. *Trends Biochem. Sci.* **31**, 276–283
20. Fitzpatrick, P.F. (2010) Oxidation of amines by flavoproteins. *Arch. Biochem. Biophys.* **493**, 13–25
21. Moustafa, I.M., Foster, S., Lyubimov, A.Y., and Vrielink, A. (2006) Crystal structure of LAAO from *Calloselasma rhodostoma* with an L-phenylalanine substrate: Insights into structure and mechanism. *J. Mol. Biol.* **364**, 991–1002
22. Faust, A., Niefind, K., Hummel, W., and Schomburg, D. (2007) The structure of a bacterial L-amino acid oxidase from *Rhodococcus opacus* gives new evidence for the hydride mechanism for dehydrogenation. *J. Mol. Biol.* **367**, 234–248
23. Coulombe, R., Yue, K.Q., Ghisla, S., and Vrielink, A. (2001) Oxygen access to the active site of cholesterol oxidase through a narrow channel is gated by an Arg-Glu pair. *J. Biol. Chem.* **276**, 30435–30441
24. Hiromoto, T., Fujiwara, S., Hosokawa, K., and Yamaguchi, H. (2006) Crystal structure of 3-hydroxybenzoate hydroxylase from comamonas testosteroni has a large tunnel for substrate and oxygen access to the active site. *J.Mol.Biol.* **364**, 878–896
25. Alfieri, A., Fersini, F., Ruangchan, N., Prongjit, M., Chaiyen, P., and Mattevi, A. (2007) Structure of the monooxygenase component of a two-component flavoprotein monooxygenase. *Proc. Natl. Acad. Sci. USA* **104**, 1177–1182
26. Kim, S.-H., Hisano, T., Takeda, K., Iwasaki, W., Ebihara, A., and Miki, K. (2007) Crystal structure of the oxygenase component (hpab) of the 4-hydroxyphenylacetate 3-monooxygenase from *Thermus thermophilus* HB8. *J. Biol. Chem.* **282**, 33107–33117
27. Baron, R., Riley, C., Chenprakhon, P., Thotsaporn, K., Winter, R.T., Alfieri, A., Forneris, F., van Berkel, W.J.H., Chaiyen, P., Fraaije, M.W., Mattevi, A., and McCammon, J.A. (2009) Multiple pathways guide oxygen diffusion into flavoenzyme active sites. *Proc. Natl. Acad. Sci. USA* **106**, 10603–10608
28. Sucharitakul, J., Prongjit, M., Haltrich, D., and Chaiyen, P. (2008) Detection of a C4a-hydro- peroxyflavin intermediate in the reaction of a flavoprotein oxidase. *Biochemistry* **47**, 8485–8490
29. Entsch, B. and Van Berkel, W.J.H. (1995) Structure and mechanism of para-hydroxybenzoate hydroxylase. *FASEB J.* **9**, 476–483
30. Koyama, H. and Suzuki, H. (1986) Spectral and kinetic studies on *Pseudomonas* L-phenylalanine oxidase (deaminating and decarboxylating). *J. Biochem.* **100**, 859–866
31. Suzuki, H., Koyama, H., Nishina, Y., Sato, K., and Shiga, K. (1991) A resonance Raman study on a reaction intermediate of *Pseudomonas* L-phenylalanine oxidase (deaminating and decarboxylating). *J. Biochem.* **110**, 169–172
32. Murshudov, G.N., Vagin, A.A., Lebedev, A., Wilson, K.S., and Dodson, E.J. (1999) Efficient anisotropic refinement of macromolecular structures using FFT. *Acta Crystallogr. D.* **55**, 247–255
33. Sheldrick, G.M. (2008) A short history of SHELX. *Acta Crystallogr. Sect. A.* **64**, 112–122
34. The PyMOL Molecular Graphics System, Version 0.99rc6, Schrödinger, LLC
35. Pettersen, E.F., Goddard, T.D., Huang, C.C., Couch, G.S., Greenblatt, D.M., Meng, E.C., and Ferrin, T.E. (2004) UCSF Chimera—a visualization system for exploratory research and analysis. *J. Comp. Chem.* **25**, 1605–1612
36. Petřk, M., Otyepka, M., Banáš, P., Košinová, P., Koča, J., and Damborský, J. (2006) CAVER: a new tool to explore routes from protein clefts, pockets and cavities. *BMC Bioinf.* **7**, 316
37. Damborský, J., Petřek, M., Banáš, P., and Otyepka, M. (2007) Identification of channels in proteins, nucleic acids, inorganic materials and molecular ensembles. *Biotechnol. J.* **2**, 62–67

38. Li, M., Binda, C., Mattevi, A., and Edmondson, D.E. (2006) Functional role of the "aromatic cage" in human monoamine oxidase B: Structures and catalytic properties of tyr435 mutant proteins. *Biochemistry* **45**, 4775–4784
39. Umhau, S., Pollegioni, L., Molla, G., Diederichs, K., Welte, W., Pilone, M.S., and Ghisla, S. (2000) The X-ray structure of D-amino acid oxidase at very high resolution identifies the chemical mechanism of flavin-dependent substrate dehydrogenation. *Proc. Natl. Acad. Sci. USA* **97**, 12463–12468
40. Porter, D.J.T. and Voet, D. (1978) The crystal structure of a flavin–nicotinamide biscoenzyme in two oxidation states. Models for flavin–nicotinamide interactions. *Acta. Crystallogr.* **B34**, 598–606
41. Sobrado, P. and Fitzpatrick, P.F. (2003) Analysis of the role of the active site residue Arg98 in the flavoprotein tryptophan 2-monooxygenase, a member of the L-amino oxidase family. *Biochemistry* **42**, 13826–13832
42. Sobrado, P. and Fitzpatrick, P.F. (2003) Identification of Tyr413 as an active site residue in the flavoprotein tryptophan 2-monooxygenase and analysis of its contribution to catalysis. *Biochemistry* **42**, 13833–13838
43. Basran, J., Sutcliffe, M.J., and Scrutton, N.S. (2001) Optimizing the Michaelis complex of trimethylamine dehydrogenase. Identification of interactions that perturb the ionization of substrate and facilitate catalysis with trimethylamine base. *J. Biol. Chem.* **276**, 42887–42892
44. Zhao, G. and Jorns, M.S. (2005) Ionization of zwitterionic amine substrates bound to monomeric sarcosine oxidase. *Biochemistry* **44**, 16866–16874
45. Dunn, R.V., Marshall, K.R., Munro, A.W., and Scrutton, N.S. (2008) The pH dependence of kinetic isotope effects in monoamine oxidase A indicates stabilization of the neutral amine in the enzyme–substrate complex. *FEBS J.* **275**, 3850–3858
46. Entsch, B., Cole, L.J., and Ballou, D.P. (2005) Protein dynamics and electrostatics in the function of *p*-hydroxybenzoate hydroxylase. *Arch. Biochem. Biophys.* **433**, 297–311
47. Ballou, D.P., Entsch, B., and Cole, L.J. (2005) Dynamics involved in catalysis by single-component and two-component aromatic hydroxylases. *Biochem. Biophys.Res. Commn.* **433**, 297–311